Low-temperature synthesis of α-alumina nanosheets on microfibrous-structured Al-fibers for Pd-catalyzed CO oxidative coupling to dimethyl oxalate

Chunzheng Wang, Weisong Xu, Zhengxing Qin, Xinmei Liu, Svetlana Mintova

Low-temperature synthesis of α-alumina nanosheets on microfibrous-structured Al-fibers for Pd-catalyzed CO oxidative coupling to dimethyl oxalate

Chunzheng Wang[a,*], Weisong Xu[a], Zhengxing Qin[a], Xinmei Liu[a], Svetlana Mintova[a,b]

[a] State Key Laboratory of Heavy Oil Processing, College of Chemical Engineering, China University of Petroleum (East China), Qingdao 266580, China

[b] Laboratoire Catalyse et Spectrochimie (LCS), Normandie Université, ENSICAEN, UNICAEN, CNRS, 6 boulevard Maréchal Juin, Caen 14050, France

[*] Corresponding author. E-mail: *czwang@upc.edu.cn*

Abstract

We reported the low-temperature synthesis of α-Al_2O_3 nanosheets on the microfibrous-structured Al-fibers at 800 $^{\circ}$C. The boehmite (AlOOH) nanosheets were initially formed on the Al-fibers through in situ endogenous growth. Then the AlOOH/Al-fibers was transformed to the α-Al_2O_3/Al-fibers composite at 800 $^{\circ}$C by a single heating step. The low-temperature phase transformation was tentatively attributed to the Al metal in the AlOOH/Al-fibers. Palladium was then dispersed on the α-Al_2O_3/Al-fibers composite, and the resulting Pd/α-Al_2O_3/Al-fibers catalyst was examined in the strongly exothermic CO oxidative coupling to dimethyl oxalate (DMO) reaction. High CO conversion of 58 % and DMO selectivity of 95 % were obtained and maintained for at least 150 h using a feedgas of CH_3ONO / CO / N_2 (1 / 1.4 / 7.6, mole) at 150 $^{\circ}$C with a gas hourly space velocity of 20000 mL g^{-1} h^{-1}. Computational fluid dynamics calculations and experimental results indicated that the Pd/α-Al_2O_3/Al-fibers catalyst remarkably decreased the hot-spot temperature of catalyst bed due to its enhanced thermal conductivity.

Keywords: Structured catalyst; Alpha alumina; Nanosheet; Phase transformation; Aluminum fiber; Dimethyl oxalate.

1. Introduction

Alpha alumina (α-Al_2O_3) is of fundamental and technological importance for plenty of applications in the petroleum industries and environmental protection [1–3]. In general, α-Al_2O_3 is derived from the thermolysis of gibbsite, boehmite, other hydrated alumina and undergoes a lot of transitional phases (η-, γ-, δ-, θ-, χ-, κ-Al_2O_3) [4,5]. However, these methods commonly require a high calcination temperature above 1100 $^{\circ}$C and thus lead to high energy consumption. This becomes a reason for developing a low-temperature synthesis procedure of α-Al_2O_3. Several groups reported on the use of additives such as seeds, oxidants, chelating agents, mineralizers and special reactors (laser or microwave) to lower the formation temperature of α-Al_2O_3 [6,7]. Suchanek et al. reported the synthesis of α-Al_2O_3 nanosheets using AlOOH under hydrothermal treatment in the presence of α-Al_2O_3 seeds and additives (H_2O_2, SiO_2 and H_3BO_3) at 380–450 ºC under 6.9–14.5 MPa [8,9].

The α-Al_2O_3-based catalysts are usually loaded in the fixed-bed reactors as randomly packed pellets of several millimeters. Such packed beds suffer from the large pressure drop, low intraparticle/interbed heat transfer and irregular flow pattern, which is detrimental to high-throughput, diffusion-determining and strongly exothermic/endothermic reactions [10,11]. To solve these problems, α-Al_2O_3 is directly manufactured into the structured foam and honeycomb monoliths, but the mechanical strength of the structure is very poor [12]. Furthermore, α-Al_2O_3 is deposited on the structured foam (Ni, Al) and honeycomb (cordierite) monoliths by coating techniques, which combines the merits of α-Al_2O_3 support with structured substances [13]. The catalysts using Al_2O_3-coated structured substances as supports, showed the high catalyst utilization and enhanced heat-transfer performance [14,15]. However, the conventional coating techniques are subjected to the nonuniformity and detachment of the coating layer as well as harmful contamination of the binder [16,17].

Recently, the conversion of non-petroleum syngas (CO/H_2) into chemicals and liquid fuels is a promising alternative to the petrochemical-based routes [18]. The gas-phase carbonylation of methyl nitrite (CH_3ONO) to dimethyl oxalate (DMO, $(CH_3OCO)_2$) is a pivotal step from syngas to ethylene glycol (DMO hydrogenation) [19]. This process is self-closing and includes chemical-looping with two main reactions: (1) Pd-catalyzed CO oxidative coupling to DMO: $2\ CH_3ONO + 2\ CO \rightarrow 2\ NO + (CH_3OCO)_2$; and (2) noncatalytic CH_3ONO regeneration: $2\ NO + 2\ CH_3OH + 1/2\ O_2 \rightarrow 2\ CH_3ONO + H_2O$. The overall reaction ($2\ CO + 2\ CH_3OH + 1/2\ O_2 \rightarrow (CH_3OCO)_2 + H_2O$) is highly efficient and environmentally benign. However, the industrial Pd/α-Al_2O_3 catalyst for CO oxidative coupling to DMO, needs a high Pd content of 2 wt.% (the-state-of-the-art), leading to a compromised economy of the DMO production [20]. The on-going efforts have been dedicated to reduce the Pd content by proper tuning of the Pd size/shape, Pd-support interactions and adding of a promoter [21–23]. Peng et al. reported a high-performance Pd/α-Al_2O_3 catalyst with Pd content of only 0.13 wt.% [22]. Nevertheless, little attention is paid to the α-Al_2O_3 support used in the strongly exothermic CO oxidative coupling to DMO ($\Delta H_{25\ ^\circ C} = -159$ kJ mol^{-1}). The real application of α-Al_2O_3 a few millimeters in size, may provoke large temperature rise with undesired hot spot in the reactor bed, which decreases the product selectivity and even makes the temperature control difficult [21,23]. To overcome this problem, a structured Pd-Fe/α-Al_2O_3-coated-cordierite catalyst was prepared, but the Pd loading was as high as 1.0 wt.% [21]. Therefore, it is important to develop a highly efficient, low Pd-loaded catalyst with enhanced heat transfer for both fundamental study and commercial application.

Herein, we revealed the low-temperature synthesis method of α-Al_2O_3 nanosheets on the microfibrous-structured Al-fibers through the phase transformation of AlOOH nanosheets at 800 $^\circ$C. Both the metal Al-promoted phase transformation of AlOOH and the formation of α-Al_2O_3 were

carefully studied. The Pd/α-Al_2O_3/Al-fibers catalyst was prepared by incipient-wetness impregnation using the as-obtained α-Al_2O_3/Al-fibers composite, and was tested in the strongly exothermic CO oxidative coupling to DMO reaction. Such microfibrous-structured catalyst showed a combination of improved heat transfer, low pressure drop, good activity, and excellent stability. The computational fluid dynamics (CFD) simulation was carried out to probe the heat-transfer ability of the microfibrous-structured catalyst.

2. Experimental

2.1. Catalyst preparation

A thin fibers felt (2.0 m length × 1.0 m width × ~1.3 mm thickness) of 60-μm Al-fibers (99.9 wt.% Al) was employed as a substrate; it was purchased from Shanghai Xincai Network-microstructured Material Co. Ltd. (China). The circular Al-fibers (8 mm diameter; equal to the internal diameter of fixed-bed reactor) were tailored from the purchased fibers felt, and treated with 0.1 wt.% NaOH solution at 25 °C for 2 min to remove the protective oxide layers from the surface. Subsequently, the pre-treated Al-fibers were loaded into a quartz tube, and oxidized in steam flow at 120 °C for 6 h to form the boehmite (AlOOH) nanosheets on the Al-fibers surface (denoted as AlOOH/Al-fibers) [24]. The as-prepared AlOOH/Al-fibers were heated to 800 °C in air with a ramping rate of 2 °C min^{-1} and kept at that temperature for 2 h to obtain the α-Al_2O_3/Al-fibers composite.

The catalysts with a theoretical Pd content of 0.3 wt.% were prepared, as described elsewhere [23]. 0.0128 g of palladium acetate ($Pd(CH_3COO)_2$, 47 wt.% Pd, Sinopharm Chemical Reagent Co., Ltd., China) was dissolved in 3.7 g of toluene ($C_6H_5CH_3$) and the solution was used to impregnate 2.0 g of the α-Al_2O_3/Al-fibers composite. After drying at 100 °C for 2 h, the pre-impregnated Al-fibers were calcined at 300 °C in air for 2 h to obtain the catalyst denoted as Pd/α-Al_2O_3/Al-fibers. For reference,

an α-Al_2O_3 (60–80 mesh; Alfa Aesar (China) Chemical Co. Ltd.) support was used to prepare the Pd/α-Al_2O_3 catalyst by the same preparation method.

2.2. Characterizations

Scanning electron microscope (SEM) observations were conducted on a Hitachi S-4800 instrument. Transmission electron microscope (TEM) images were obtained with a FEI TECNAI G^2 F30 instrument at 300 kV. The shell of the α-Al_2O_3/Al-fibers composite was carefully removed by a cutter knife and then the obtained powder (i.e., the shell) was used for the TEM analysis. X-ray diffraction (XRD) patterns of samples were recorded on a Rigaku Ultima IV diffractometer with Cu Kα radiation (35 kV and 25 mA). Diffuse reflectance infrared Fourier transform spectroscopy (DRIFTS) spectra were recorded in a Bruker Tensor 27 spectrometer equipped with a Harrick Scientific HVC-DRP-4 cell and a liquid N_2 cooled mercury-cadmium-telluride (MCT) detector. The actual Pd loading was measured using inductively coupled plasma-atomic emission spectroscopy (ICP-AES) with a Thermo IRIS Intrepid II XSP apparatus. Prior to the analysis, the sample was dissolved in aqua regia. Pd ICP standard solutions with concentrations of 5, 10 and 20 $\mu g\ g^{-1}$ were used to obtain the calibration curve. Nitrogen physisorption was performed at −196 $^{\circ}$C using a Quantachrome Quadrasorb-evo instrument. The specific surface area and pore size distribution were estimated using the Brunauer-Emmett-Teller (BET) theory and Barrett-Joyner-Halenda (BJH) method based on the desorption branch of the isotherms. X-ray photoelectron spectroscopy (XPS) spectra were obtained on an Escalab 250xi spectrometer with an analyzer pass energy of 30.0 eV and an Al Kα X-ray source (300 W). The results were referenced to the adventitious carbon, C1s peak at 284.6 eV prior to fitting the spectra. H_2-temperature programmed reduction (H_2-TPR) was conducted on a Tianjin XQ TP-5080 apparatus equipped with a thermal conductivity detector (TCD). 100 mg of sample was treated with He (flow of

40 mL min^{-1}) at 300 °C for 1 h and then cooled to 25 °C. Subsequently, a gas mixture of 5 vol.% H_2/N_2 was introduced into the reactor at 40 mL min^{-1}. After the baseline of TCD signal was steady, the sample was heated to 300 °C at 10 °C min^{-1}.

2.3. Catalytic tests

The catalytic behavior of the Pd/α-Al_2O_3/Al-fibers and Pd/α-Al_2O_3 catalysts was tested in a vertical fixed-bed, continuous down-flow quartz tube microreactor (internal diameter of 8 mm, length of 760 mm) (Scheme 1) [25]. Three calibrated mass flow controllers were employed to regulate the flow rates of N_2, CO, the gas mixture of methyl nitrite (CH_3ONO) and N_2. The weight of the catalyst was 0.12 g at gas hourly space velocity (GHSV) of 20000 mL g^{-1} h^{-1} and 0.04 g at GHSV of 60000 mL g^{-1} h^{-1}. The reaction temperature was varied in the range of 120–200 °C. Prior to the test, the catalyst was in situ activated by performing the CO oxidative coupling to DMO at 200 °C for 2 h with a gas mixture of CH_3ONO / CO / N_2 (1 / 1.4 / 7.6, mole) [23]. The outlet gas was analyzed by an on-line gas chromatography (GC; Shanghai Ouhua 9160, China) equipped with a thermal conductivity detector (TCD) and flame ionization detector (FID). The TCD and FID were connected to a ShinCarbon ST packed column (DIKMA) and Innowax PEG-20M capillary column (HP), respectively. The six-way valve for FID and partial gas pipelines were heated at 120 °C to avoid the condensation of reaction products. The calculations of the turnover frequency (TOF), CO conversion, DMO selectivity and "methanol + methyl formate" (ME + MF) selectivity were presented in the Supporting Information.

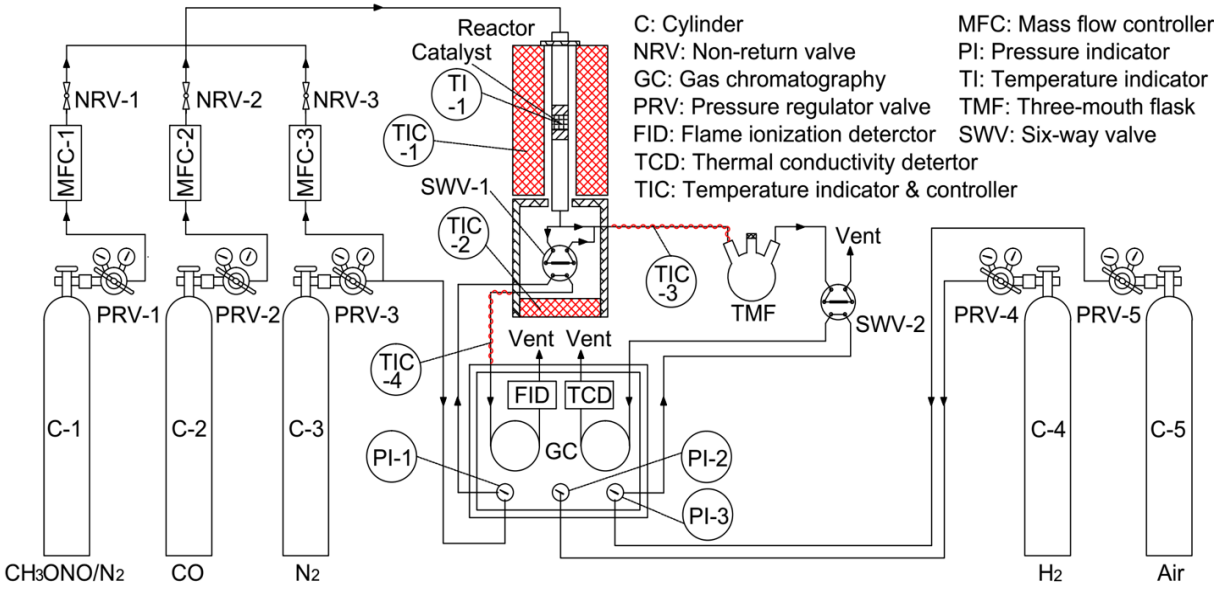

Scheme 1. Schematic diagram of the apparatus used for catalyst testing (the red parts are heated).

3. Results and discussion

3.1. Low-temperature synthesis of α-Al_2O_3 nanosheets on microfibrous-structured Al-fibers

3.1.1. Feature of α-Al_2O_3/Al-fibers composite

Figure 1A schematically illustrates the endogenous growth of AlOOH nanosheets on the microfibrous-structured Al-fibers and the subsequent formation of α-Al_2O_3 nanosheets by low-temperature treatment (calcination). Circular Al-fibers with entirely open three-dimensional (3D) network, consisting of 10 vol.% 60-μm Al-fibers and 90 vol.% void volume were employed as the pristine substrate (Fig. 1B). The Al-fibers had a smooth surface as shown in the SEM images (Fig. S1). With the aid of the steam-only oxidation between Al metal and H_2O at 120 °C (2 Al + 4 H_2O → 2 AlOOH + 3 H_2), the uniform and honeycomb-like AlOOH nanosheets were endogenously generated, and aligned to a nanosheet array (shell) on the Al-fibers (core) (Fig. 1C) [24]. The thickness of the AlOOH shell was about 0.7 μm (inset of Fig. 1C) corresponding to an AlOOH content of 7.5 wt.% [24]. The as-prepared AlOOH/Al-fibers composite was calcined in air at 800 °C. The nanosheets were

preserved (Fig. 1D) but the microstructure of these nanosheets was slightly changed, possibly due to the dehydroxylation of the AlOOH (Fig. S2). It should be noted that the metal Al (core) could not leak from the core-shell AlOOH/Al-fibers composite even at high-temperature treatment at 800 $^{\circ}$C (melting point of Al is 660 $^{\circ}$C), due to the obstruction of densely packed AlOOH nanosheets (shell). The similar observations were obtained on the Al alloys (Ni-Al and Fe-Al), indicating that the protective alumina scale on the alloys surface could provide excellent oxidation resistance above 1000 $^{\circ}$C [26-28]. The characteristic diffraction peaks of metal Al (JCPDS 04-0787) were clearly observed in the pristine Al-fibers (Fig. 1E, pattern a). The weak diffraction peaks at 28.2 and 49.3° 2 theta were attributed to the boehmite (JCPDS 21-1307) (Fig. 1E, pattern b). After the calcination at 800 $^{\circ}$C, the α-Al_2O_3/Al-fibers composite showed the formation of α-Al_2O_3 phase (JCPDS 10-0173) confirmed by the appearance of the diffraction peaks at 25.6, 35.1, 43.4, 52.6, 57.5, 66.5 and 68.2° 2 theta (Fig. 1E, pattern c). In addition, the DRIFTS spectrum of AlOOH/Al-fibers composite contained five bands at 3336, 3126, 1066, 857 and 788 cm^{-1} that correspond to boehmite (Fig. 1F). The broad bands in the region 3600–3100 cm^{-1} were assigned to O-H stretching vibrations of water, while the bands at 950–600 cm^{-1} are the Al-O bending stretching mode of α-Al_2O_3 [29,30]. The DRIFTS results were in a good agreement with the XRD results. The as-prepared α-Al_2O_3/Al-fibers composite had a BET specific surface area of 4.0 $m^2\ g^{-1}$ and a total pore volume of 0.012 $cm^3\ g^{-1}$ (including the Al-fibers) (Fig. 1G). After the Al-fibers content of ~93 wt.% was subtracted, it was calculated that the α-Al_2O_3 shell had a large BET surface area of ~50.0 $m^2\ g_{\alpha\text{-}Al_2O_3}{}^{-1}$ and total pore volume of ~0.150 $cm^3\ g_{\alpha\text{-}Al_2O_3}{}^{-1}$. The α-Al_2O_3/Al-fibers composite displayed a type-Ⅳ isotherm and mesopores with a size in the range of 4–19 nm. The appearance of type-H3 hysteresis loop at $P/P_0 > 0.5$ was attributed to the voids formed by stacking of α-Al_2O_3 nanosheets (Fig. 1G).

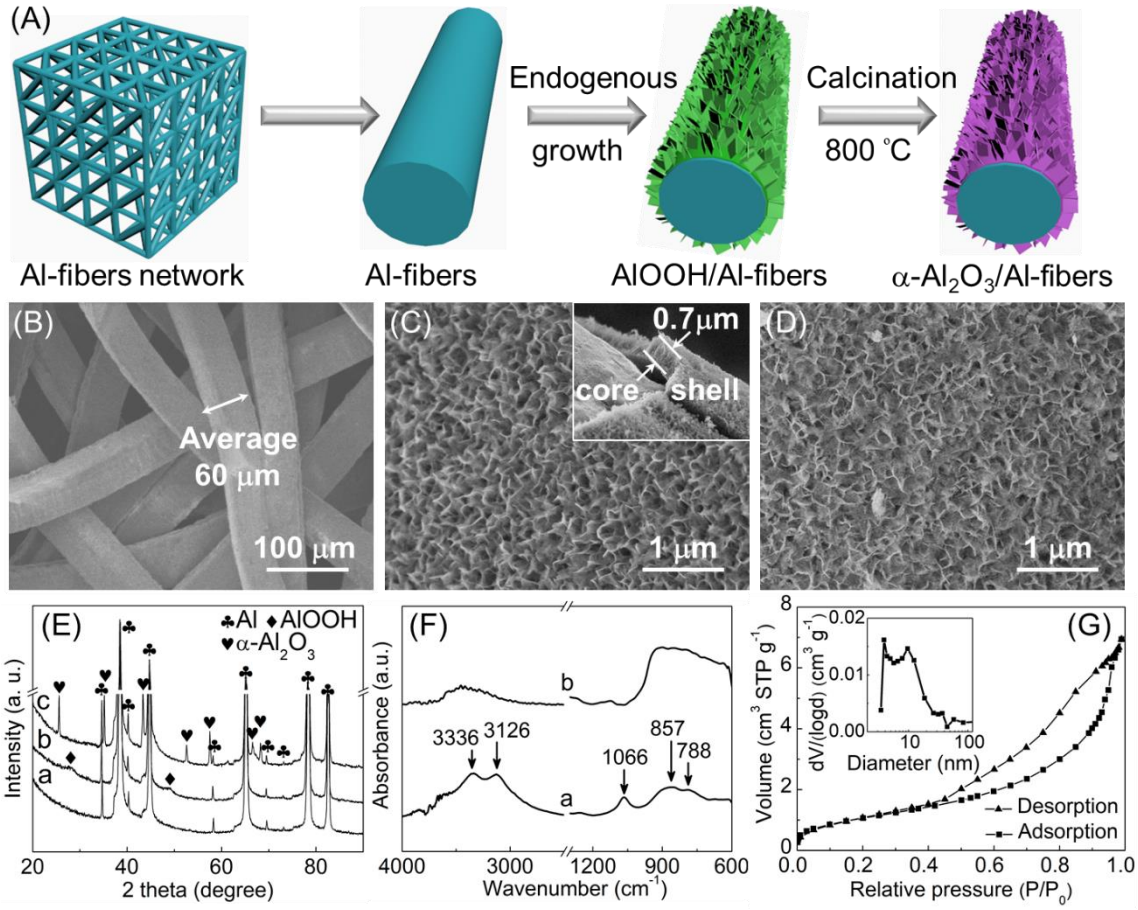

Fig. 1. (A) Schematic presentation of the top-down strategy applied for preparation of the core-shell α-Al_2O_3/Al-fibers composite. SEM images of (B) microfibrous-structured Al-fibers, (C) AlOOH/Al-fibers (*Inset*: core(Al-fibers)-shell(AlOOH) structure) and (D) α-Al_2O_3/Al-fibers composite. (E) XRD patterns of the (a) Al-fibers substrate, (b) AlOOH/Al-fibers and (c) α-Al_2O_3/Al-fibers composite. (F) DRIFTS spectra of (a) AlOOH/Al-fibers and (b) α-Al_2O_3/Al-fibers composite, and (G) N_2 sorption isotherm of the α-Al_2O_3/Al-fibers composite (*Inset*: BJH mesopore size distribution obtained from the desorption branch of the isotherm).

The shell of the α-Al_2O_3/Al-fibers composite was carefully removed by a cutter knife and the obtained powder (the shell) was analyzed by TEM (Fig. 2). TEM images showed that the shell of the α-Al_2O_3/Al-fibers composite was composed of nanosheets (Fig. 2A). This observation was in

agreement with the nanosheet array observed in the SEM image (Fig. 1D). The nanosheets structure remained intact after calcination at 800 °C, indicating the good thermal stability. The thickness of the nanosheets was 2–6 nm as measured by TEM (Fig. 2A). From the HRTEM image, the lattice spacing of the nanosheets of 0.25 nm was calculated, which possibly corresponds to the (104) lattice plane of α-Al_2O_3 crystals (JCPDS 10-0173). This result further verified the formation of α-Al_2O_3 on the α-Al_2O_3/Al-fibers composite, which was consistent with the XRD and DRIFTS results (Fig. 1E and Fig. 1F).

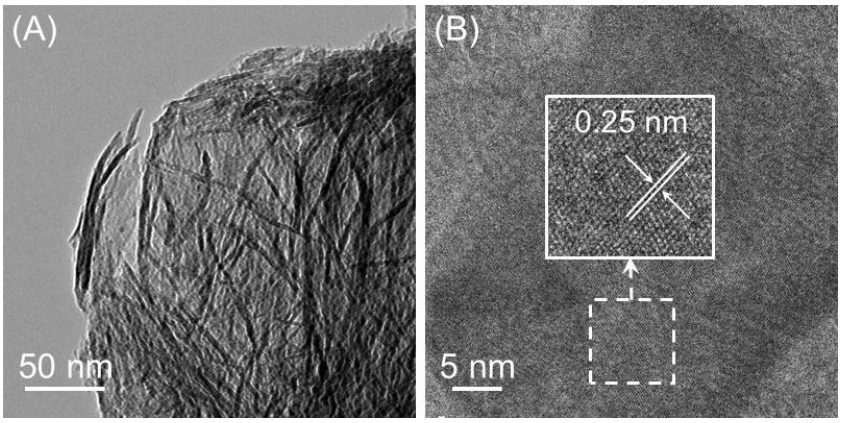

Fig. 2. TEM images of the α-Al_2O_3/Al-fibers composite: (A) scale bar, M = 50 nm and (B) scale bar, M = 5 nm (*Inset:* enlarged area of the composite with a lattice spacing of the nanosheets of 0.25 nm).

3.1.2. Phase transformation of AlOOH in the Al-fibers

Fig. 3 shows the XRD patterns of the AlOOH/Al-fibers composite calcined at various temperatures. After calcination at 600 °C, the diffraction peaks at 45.8 and 67.1° 2 theta were assigned to γ-Al_2O_3 (JCPDS 80-0956) (Fig. 3, pattern a). This revealed that the AlOOH on the Al-fibers could convert to γ-Al_2O_3 at 600 °C. The peak intensity of 67.1° 2 theta increased gradually but the γ-Al_2O_3 phase remained unchanged with arising the calcination temperature from 600 to 750 °C (Fig. 3, patterns a–c). However, the AlOOH on the Al-fibers was transformed into α-Al_2O_3 at 800 °C (Fig. 3, pattern d). The

composite after calcination at 600 °C was calcined again at 800 °C, and the XRD pattern was identical with that of the composite calcined at 800 °C (Fig. 3, patterns d,e). This suggested that the γ-Al_2O_3 on the Al-fibers converted to α-Al_2O_3 at 800 °C. This result confirmed that the AlOOH on the Al-fibers is transformed according to the following scheme: AlOOH → γ-Al_2O_3 → α-Al_2O_3.

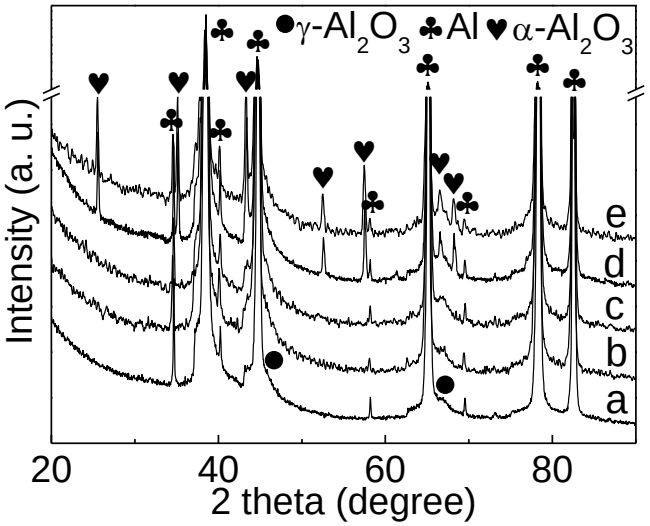

Fig. 3. XRD patterns of the AlOOH/Al-fibers composite after calcination: (a) 600 °C for 2 h, (b) 700 °C for 2 h, (c) 750 °C for 2 h, (d) 800 °C for 2 h, (e) 600 °C for 2 h and subsequent 800 °C for 2 h.

Fig. 4 shows the XPS spectra of the Al 2p and O 1s regions for the AlOOH/Al-fibers composite before and after calcination. As shown in Fig. 4A, these four composites had a binding energy (BE) of 74.0–74.6 eV, which was attributed to Al^{3+} in alumina [31]. The absence of Al 2p peak at 72.5 eV indicated that the Al-Al bond (Al metal) was not present on the surface of these four composites [32]. This further confirmed the SEM observation that the metal Al could not leak from the Al-fibers under calcination at 800 °C (Fig. 1D). The full width at half-maximum (FWHM) of Al 2p peak on the AlOOH/Al-fibers (1.5 eV) without calcination was lower than of the other three composites (2.0–2.3 eV) (Fig. 4A and Table 1). The Al 2p peak with a characteristic FWHM of 1.5 eV was attributed to boehmite [33], suggesting the presence of AlOOH on the surface of the AlOOH/Al-fibers. This result

was consistent with the XRD and DRIFTS results (Fig. 1E and 1F). As shown in Fig. 4B, the broad O 1s spectra were decomposed into two component species: Al-O (530.7 eV) and Al-OH (532.1 eV) [34,35]. From the XPS results one can see that the peak area ratio of Al-O and Al-OH gradually increased, due to the desorption of hydroxyl groups at high temperature (Fig. 4B and Table 1).

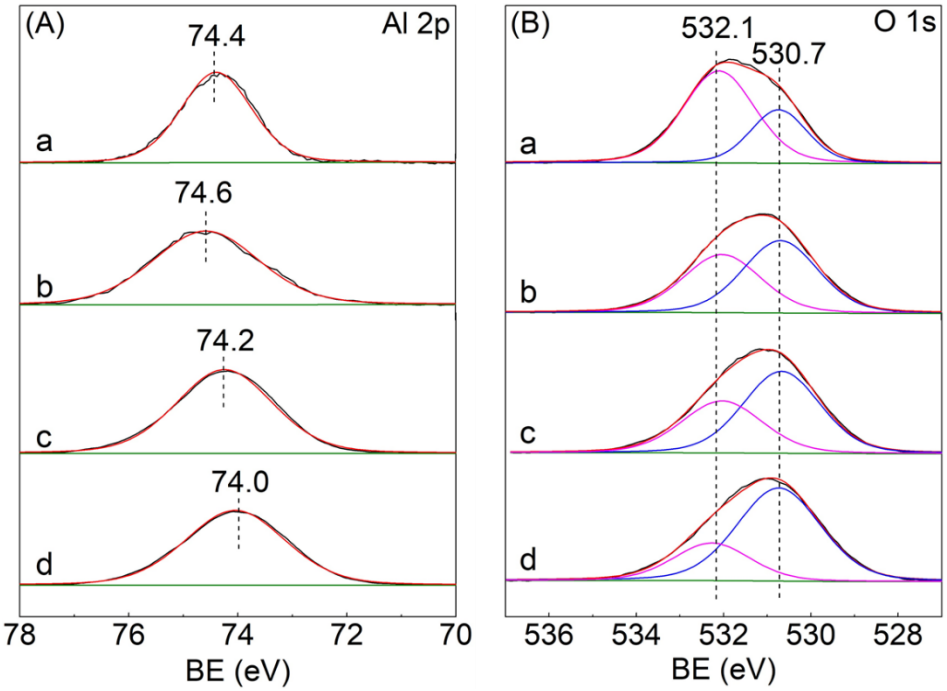

Fig. 4. XPS spectra of (A) Al 2p and (B) O 1s regions of the AlOOH/Al-fibers composite (a) without calcination and after calcination for 2 h at (b) 600 °C, (c) 700 °C and (d) 800 °C; the XPS peaks were deconvoluted using the Gaussian-Lorentzian sum function and Newton iteration method after a linear background subtraction.

Table 1. Parameters obtained from the XPS spectra[a].

Sample[a]	Al 2p		O 1s at 530.7 eV		O 1s at 532.1 eV		O 1s
	BE (eV)	FWHM (eV)	FWHM (eV)	Area	FWHM (eV)	Area	Ratio[b]
a	74.4	1.5	1.9	738	1.5	1584	0.46

b	74.6	2.3	2.1	1172	2.0	977	1.20
c	74.2	2.0	2.2	1313	2.1	771	1.70
d	74.0	2.1	2.1	1489	2.3	549	2.71

[a] XPS spectra of the AlOOH/Al-fibers composite without calcination (a) and after calcination for 2 h at (b) 600 °C, (c) 700 °C and (d) 800 °C.

[b] Area ratio of O 1s peak at 530.7 eV to the peak at 532.1 eV.

3.1.3. Low-temperature synthesis of α-Al_2O_3: promotion of Al metal

The low-temperature phase transformation from AlOOH to α-Al_2O_3 was initially attributed to the presence of Al metal. Firstly, reference AlOOH nanosheets were synthesized from a bayerite precursor as described elsewhere (Fig. 5A, pattern a) [36]. Even though the average thickness of the reference AlOOH nanosheets (1–5 nm measured by TEM images) was similar to the counterpart of nanosheets of the AlOOH/Al-fibers (Fig. 2A) [36], the former was totally transformed into γ-Al_2O_3 after calcination at 800 °C (Fig. 5A, pattern b). This was consistent with the previous reports revealing that the boehmite could not convert to α-Al_2O_3 at 800 °C [37,38]. Secondly, to study the effect of the Al metal, the AlOOH/Al-fibers composite calcined at 600 °C was treated with an excess of NaOH solution (4.0 wt.%) to remove the Al metal. Note that the concentration of NaOH solution should be carefully controlled, otherwise the composite will be completely dissolved in a concentrated solution. After the treatment, the rest of the AlOOH/Al-fibers composite calcined at 600 °C showed the characteristic diffraction peaks corresponding to the γ-Al_2O_3 phase (Fig. 5B, pattern a). The rest of the AlOOH/Al-fibers composite after the calcination at 600 °C and the subsequent NaOH treatment, was treated at 800 °C but the γ-Al_2O_3 crystalline phase remained (Fig. 5B, pattern b). Both γ-Al_2O_3 and AlOOH on the Al-fibers could transform to the α-Al_2O_3 at 800 °C as previously stated (Fig. 3, patterns d,e) while only the γ-Al_2O_3 without the Al-fibers could not (Fig. 5B). The phase transformation to α-Al_2O_3 is governed

by nucleation and grain growth mechanism [39,40]. It has been confirmed experimentally and by modeling that the α-Al_2O_3 can be formed at low temperature (900–1100 °C) on Al alloys such as Fe-Al and Ni-Al, due to the promoted α-Al_2O_3 nucleation at the oxide/metal interface [7,41]. It is thus reasonable to infer that the formation of α-Al_2O_3 at 800 °C was possibly attributed to the Al metal in the AlOOH/Al-fibers composite, which lowered the nucleation energy barrier of α-Al_2O_3 at the oxide/Al metal interface.

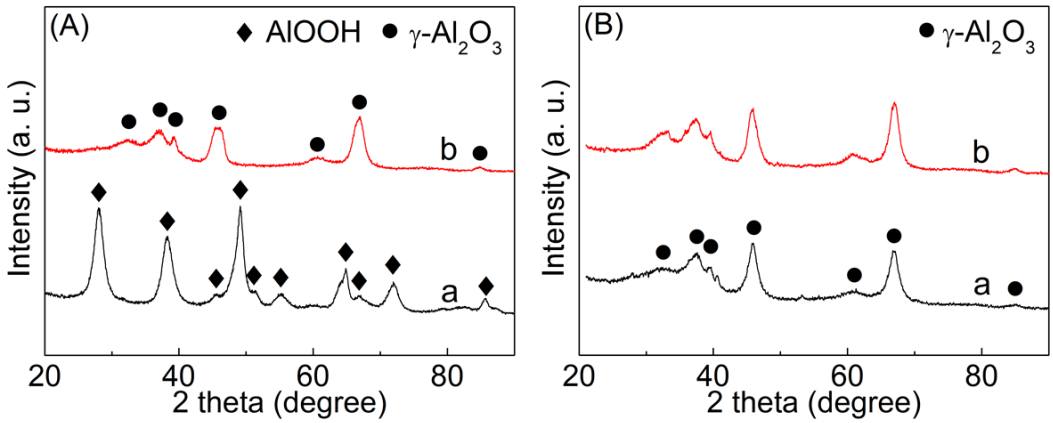

Fig. 5. (A) XRD patterns of the reference boehmite nanosheets (a) before and (b) after calcination at 800 °C. (B) XRD patterns of AlOOH/Al-fibers composite (a) calcined at 600 °C for 2 h and then treated with an excess of NaOH solution (4.0 wt.%) for 24 h, and (b) calcined at 600 °C, treated with NaOH solution and then calcined at 800 °C for 2 h.

3.2. Microfibrous-structured Pd/α-Al_2O_3/Al-fibers catalyst for CO oxidative coupling to DMO

3.2.1. Features of Pd/α-Al_2O_3/Al-fibers catalyst

The Pd/α-Al_2O_3/Al-fibers catalyst was prepared by incipient-wetness impregnation method using the as-prepared α-Al_2O_3/Al-fibers as support. As shown in Fig. 6A, the nanosheet array of α-Al_2O_3 was well retained after the Pd loading. No diffraction peaks of PdO (JCPDS 88-2434) and Pd (JCPDS 01-1201) were detectable except the peaks corresponding to Al and α-Al_2O_3, possibly due to a good

Pd dispersion (Fig. 6B). In fact, the Pd was homogeneously dispersed on the α-Al_2O_3/Al-fibers composite, with an average particle size of 4.4 ± 0.9 nm (Fig. 6C). The stacks of nanosheets of the catalyst were clearly observed, consistent with the catalyst support (Fig. 2A and Fig. 6C). The Pd/α-Al_2O_3/Al-fibers catalyst contains mesopores with a size of 4–19 nm and the BET specific surface area is 3.9 m^2 g^{-1} with a total pore volume of 0.011 cm^3 g^{-1} (including the Al-fibers mass), which were almost equal to the α-Al_2O_3/Al-fibers composite (Fig. 1G and Fig. 6D).

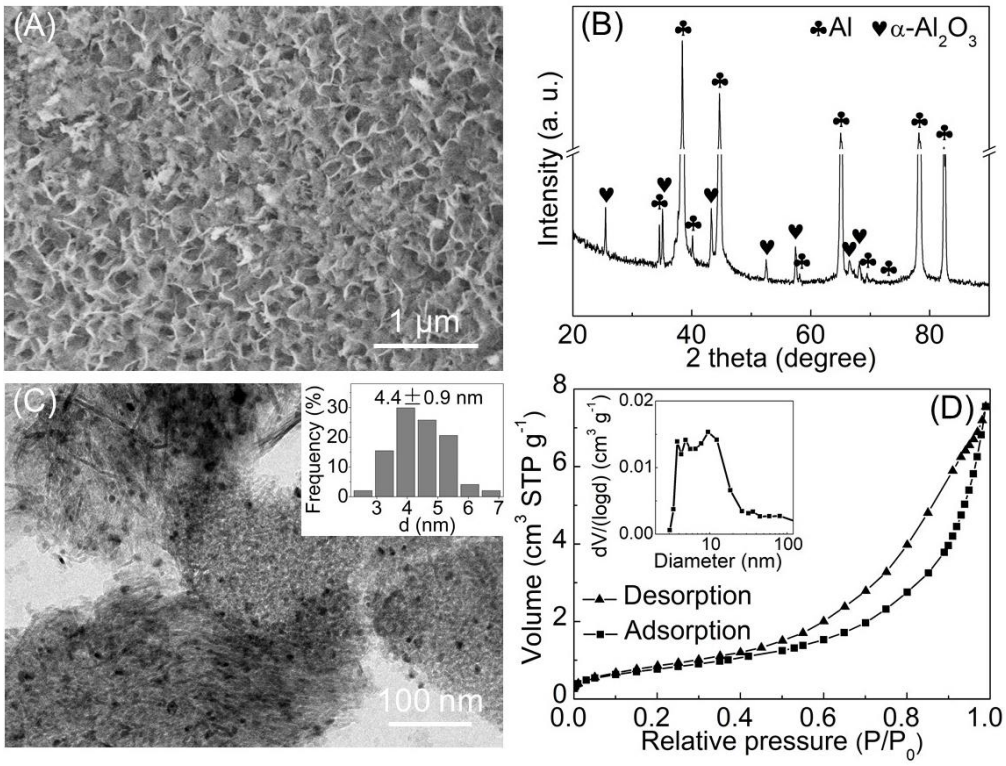

Fig. 6. (A) SEM image, (B) XRD pattern, (C) TEM image and (D) N_2 sorption isotherm (*Inset*: BJH mesopore size distribution obtained from the desorption branch of the isotherms) of the Pd/α-Al_2O_3/Al-fibers catalyst.

3.2.2. Catalytic performance of Pd/α-Al_2O_3/Al-fibers catalyst

The microfibrous-structured Pd/α-Al_2O_3/Al-fibers catalyst was tested in the CO oxidative coupling to DMO using a GHSV of 20000 mL g^{-1} h^{-1} and a feedgas of CH_3ONO / CO / N_2 (1 / 1.4 / 7.6, mole). Compared to the reference catalyst of Pd/α-Al_2O_3, the Pd/α-Al_2O_3/Al-fibers delivered similar CO

conversion, DMO selectivity and "methanol + methyl formate" (ME + MF) selectivity in the range of 120–140 °C (Fig. 7). Interestingly, the Pd/α-Al_2O_3/Al-fibers showed higher CO conversion, DMO selectivity, and lower "ME + MF" selectivity than the reference Pd/α-Al_2O_3 catalyst at temperatures ranging from 150 to 170 °C (Fig. 7). This evolution behavior was initially assigned to the different thermal conductivity of microfibrous-structured Al-fibers and the α-Al_2O_3. It should be pointed out that the CO oxidative coupling to DMO is highly exothermic ($\Delta H_{25\ ^\circ C}$ = –169 kJ mol^{-1}), which may induce large temperature rise with unexpected hot spot in the reactor bed [23]. To examine the reaction heat effect, the thermocouple was inserted in the upper side of the catalyst bed. For example, the temperature rise detected (the temperature obtained from the thermocouple minus the reactor wall temperature of 150 °C) was 5 °C on the Pd/α-Al_2O_3/Al-fibers catalyst and 11 °C on the Pd/α-Al_2O_3 catalyst. The decomposition of the CH_3ONO reactant (4 $CH_3ONO \rightarrow CH_3OCHO + 2\ CH_3OH + 4\ NO$) was very sensitive to the reaction temperature [42,43], and was boosted in the range of 150–170 °C on the Pd/α-Al_2O_3 catalyst. It was concluded that the low temperature rise inhibited the inefficient decomposition of the CH_3ONO reactant and thus led to the enhanced activity on the Pd/α-Al_2O_3/Al-fibers catalyst. Clearly, our Pd/α-Al_2O_3/Al-fibers catalyst exhibited better conversion and selectivity at high temperature of 150–170 °C, which would be an advantageous feature compared to the reference Pd/α-Al_2O_3 catalyst, by considering the strong exothermicity of the CO oxidative coupling to DMO.

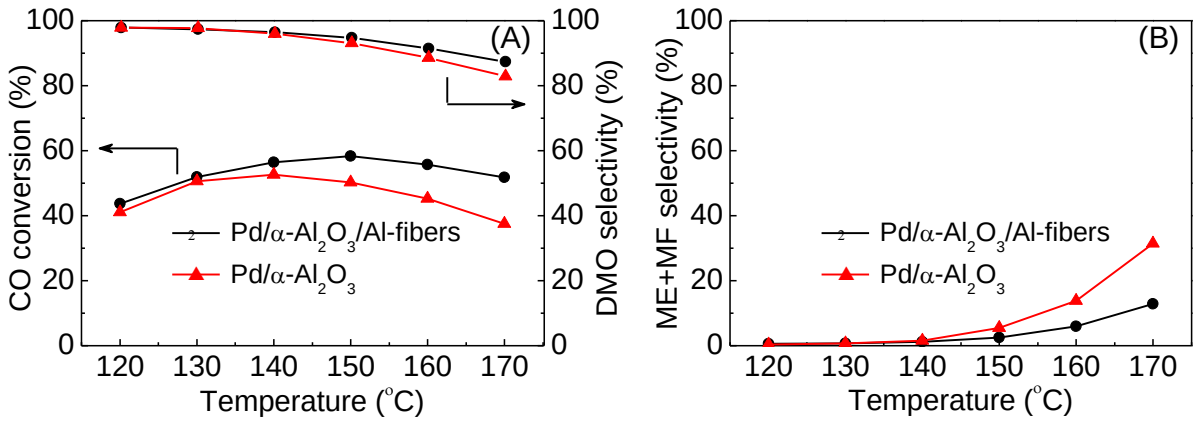

Fig. 7. (A) CO conversion, DMO selectivity and (B) "methanol + methyl formate" (ME + MF) selectivity for temperature-dependent CO oxidative coupling to DMO on the Pd/α-Al_2O_3/Al-fibers and Pd/α-Al_2O_3 catalysts. Reaction conditions: 0.12 g catalyst, CH_3ONO / CO / N_2 = 1 / 1.4 / 7.6 (mole), GHSV = 20000 mL g^{-1} h^{-1}, 1 bar. Each point was an average of 3 measurements conducted. The DMO and "ME + MF" selectivity were based on the CO and CH_3ONO, respectively (details were provided in the Supporting Information).

The catalyst characteristics and intrinsic activity (i.e., TOF) of the Pd/α-Al_2O_3/Al-fibers and Pd/α-Al_2O_3 were summarized in Table 2. The Pd loadings of the two catalysts were determined to be 0.25 wt.% and 0.26 wt.% by ICP-AES analysis. The average Pd particle sizes (*d*) in the Pd/α-Al_2O_3/Al-fibers and Pd/α-Al_2O_3 were 4.4 nm and 2.0 nm (TEM images in Fig. 6C and Fig. S3), corresponding to the Pd dispersion (*D*) of 0.25 and 0.56, respectively (the *D* was calculated using the formula $D = 1.12 / d$ [23]. Similar H_2-temperature programmed reduction (TPR) curves for the two catalysts were measured, which showed the catalysts could be completely reduced at about 120 °C (Fig. S4). As a control experiment, the CO conversion was decreased to be < 6% at 120 °C and GHSV of 60000 mL g^{-1} h^{-1} for the TOF calculation. The TOFs of 0.7 and 0.5 s^{-1} for the two catalysts, respectively were obtained, indicating comparable intrinsic activity. Clearly, the Pd/α-Al_2O_3/Al-fibers and Pd/α-Al_2O_3 catalysts have similar Pd contents, reduction behavior, comparable Pd particle size and intrinsic activity. These results suggested that the α-Al_2O_3/Al-fibers composite is a promising alternative to the conventional α-Al_2O_3 for the CO oxidative coupling to DMO.

Table 2 Content, property and activity of the Pd/α-Al_2O_3/Al-fibers and Pd/α-Al_2O_3 catalysts[a].

Sample	Pd (wt.%)[b]	*d* (nm)[c]	*D*[c]	Surface Pd (mol $g_{cat.}^{-1}$)[d]	TOF (s^{-1})[e]

Pd/α-Al_2O_3/Al-fibers	0.25	4.4	0.25	6.6×10^{-6}	0.7
Pd/α-Al_2O_3	0.26	2.0	0.56	1.4×10^{-5}	0.5

[a]Reaction conditions: 0.04 g catalyst, 120 °C, GHSV = 60000 mL g^{-1} h^{-1}, CH_3ONO / CO / N_2 = 1 / 1.4 / 7.6 (mole), 1 bar.

[b]Pd content determined by ICP-AES analysis.

[c]Pd particle size (*d*) obtained from TEM images in Fig. 6C and Fig. S3, and Pd dispersion (*D*) calculated by the formula: $D = 1.12 / d$ [23].

[d] Surface Pd atoms determined by Pd dispersion (*D*) and Pd content.

[e] TOF based on the CO conversion and surface Pd atoms.

3.2.3. Heat transfer enhancement

As previously stated, our main efforts were focused on the development of a microfibrous-structured catalyst with a combination of high catalytic performance and excellent thermal conductivity. To probe the heat-transfer ability of our catalyst, the R was conducted to obtain the temperature distribution in the microfibrous-structured bed of Pd/α-Al_2O_3/Al-fibers and randomly packed bed of Pd/α-Al_2O_3 catalysts. As shown in Fig. 8A, the tubular reactor was divided into three parts: one isothermal section and two adiabatic sections. The detailed CFD model and calculation methods were described in the Supporting Information. Fig. 8B shows the steady-state temperature distribution on the microfibrous-structured Pd/α-Al_2O_3/Al-fibers and the Pd/α-Al_2O_3 catalysts. The released reaction heat on the two catalysts was similar due to the comparable CO conversion (58 % vs. 50 % at 150 °C, Fig. 7A) under identical reaction conditions. However, the reactor' temperature distribution of the Pd/α-Al_2O_3/Al-fibers was more homogeneous than of the Pd/α-Al_2O_3 (Fig. 8B); the former showed a

hot spot with a temperature rise of 8 °C, which was much lower than the latter of 30 °C (the highest temperature of CFD simulation minus the reactor wall temperature of 150 °C). The low temperature rise for the Pd/α-Al_2O_3/Al-fibers catalyst was unambiguously attributed to the high thermal conductivity of the microfibrous-structured Al-fibers, which rapidly dissipated a large amount of reaction heat [44,45]. Notably, the trend of temperature rise by CFD simulation was consistent with the experimental observation using a thermocouple (5 vs. 8 °C on the Pd/α-Al_2O_3/Al-fibers catalyst; 11 vs. 30 °C on the Pd/α-Al_2O_3 reference catalyst).

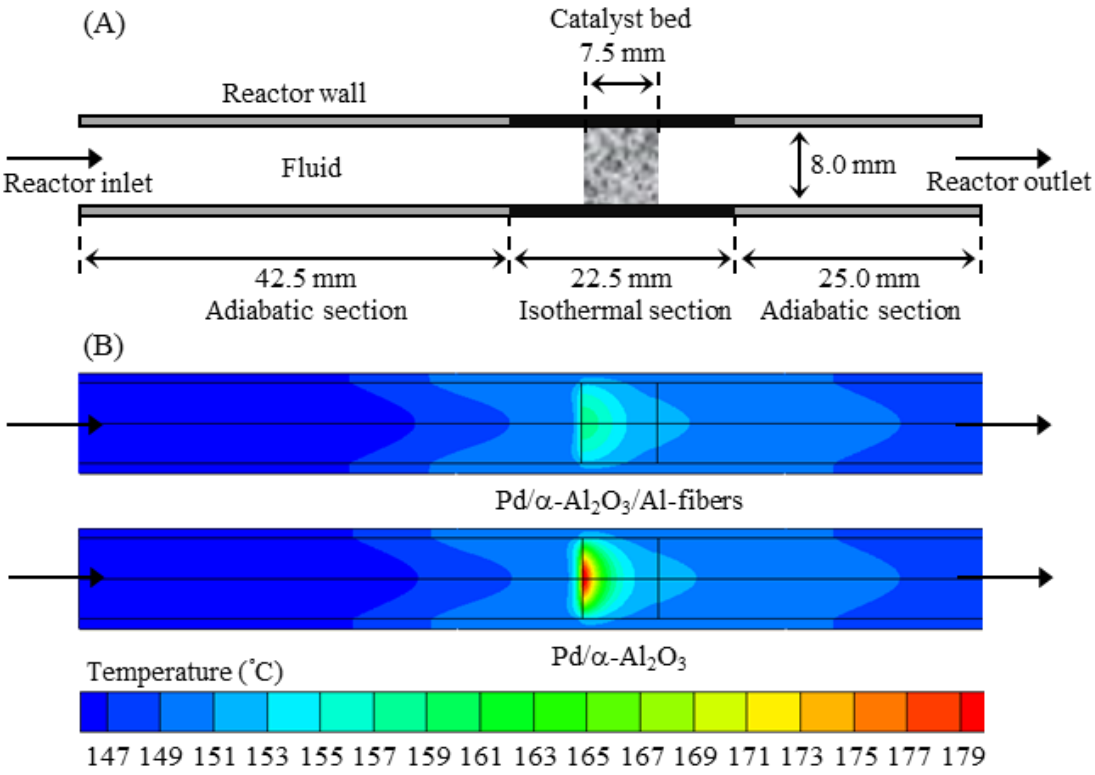

Fig. 8. (A) Schematic diagram of the system for CFD calculation, and (B) reactor temperature distribution obtained by the steady-state CFD simulation on the Pd/α-Al_2O_3/Al-fibers catalyst and reference Pd/α-Al_2O_3 catalyst.

3.2.4. Stability

To investigate the long-term stability of the catalyst, an experiment was run at 150 °C for 150 h on

the microfibrous-structured Pd/α-Al_2O_3/Al-fibers catalyst. The catalyst showed a good stability throughout the 150 h test, exhibiting a CO conversion of ~58% and DMO selectivity of ~95% (Fig. 9A). The diffraction peaks of PdO (JCPDS 88-2434) and Pd (JCPDS 01-1201) were still not detectable for the used catalyst after 150 h test (Fig. S5). The TEM image showed Pd nanoparticles with an average size of 4.5 ± 0.6 nm (Fig. S6), almost equal to that of the catalyst before the test (4.4 ± 0.9 nm, Fig. 6C). This suggested that the Pd/α-Al_2O_3/Al-fibers catalyst was resistant to the sintering of Pd nanoparticles. A noteworthy feature of the used catalyst was that the nanosheet array of α-Al_2O_3 remained unaltered, confirmed by SEM (Fig. 9B,C) and XRD (Fig. S5) characterizations.

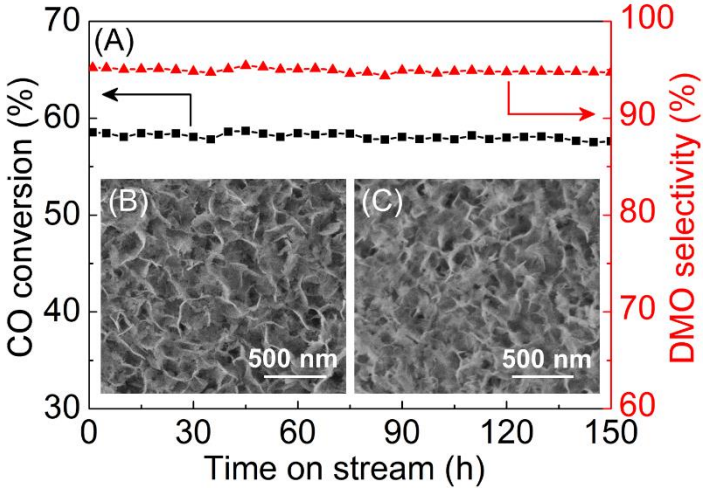

Fig. 9. (A) Durability performance of the Pd/α-Al_2O_3/Al-fibers catalyst, and SEM images of (B) fresh and (C) used Pd/α-Al_2O_3/Al-fibers catalyst after 150 h test. Reaction conditions: 0.12 g catalyst, CH_3ONO / CO / N_2 = 1 / 1.4 / 7.6 (mole), GHSV = 20000 mL g^{-1} h^{-1}, 150 °C, 1 bar. Each point was an average of 5 measurements conducted.

4. Conclusions

The α-Al_2O_3 nanosheets on the microfibrous-structured Al-fibers have been prepared through the phase transformation of boehmite nanosheets at temperature as low as 800 °C. The presence of Al metal

in the Al-fibers is responsible for the low-temperature phase transformation to α-Al_2O_3. Such α-Al_2O_3/Al-fibers, with enhanced heat transfer and low pressure drop, is a promising alternative to the conventional α-Al_2O_3 support in some industrial and environmental catalysis. As an example, the Pd/α-Al_2O_3/Al-fibers catalyst is prepared via incipient-wetness impregnation, and tested in the strongly exothermic CO oxidative coupling to dimethyl oxalate (DMO). The catalyst with a low Pd loading of 0.25 wt.% exhibits a CO conversion of 58 % and DMO selectivity of 95 % with a feedgas of CH_3ONO / CO / N_2 (1 / 1.4 / 7.6, mole) at 150 °C with a large gas hourly space velocity of 20000 mL g^{-1} h^{-1}. The Pd/α-Al_2O_3/Al-fibers catalyst showed high stability during the continuous test of 150 h. The Pd/α-Al_2O_3/Al-fibers catalyst effectively inhibited the side reaction and showed a higher activity compared to the conventional Pd/α-Al_2O_3 catalyst, resulted from the decreased temperature of the catalyst bed. Furthermore, computational fluid dynamics calculations and experimental measurements demonstrated the large reduction of hot-spot temperature thanks to the enhanced thermal conductivity originated from the microfibrous-structured Al-fibers.

Acknowledgements

This work was supported by the China Postdoctoral Science Foundation (2017M622311), Natural Science Foundation of China (21706285), Fundamental Research Funds for the Central Universities (18CX02148A, 18CX02013A), Postdoctoral Research Project of Qingdao (BY20170209) and the Sino-French International Laboratory (LIA) “Zeolites”.

References

[1] J.E. van den Reijen, S. Kanungo, T.A.J. Welling, M. Versluijs-Helder, T.A. Nijhuis, K.P. de Jong, P.E. de Jongh, J. Catal. 356 (2017) 65–74.

[2] E. Okon, H. Shehu, E. Gobina, Catal. Today 310 (2018) 146–156.

[3] S. Gudyka, G. Grzybek, J. Gryboś, P. Indyka, B. Leszczyński, A. Kotarba, Z. Sojka, Appl. Catal. B 201 (2017) 339–347.

[4] P. Pardo, J. Alarcón, Ceram. Int. 44 (2018) 11486–11496.

[5] E. Rytter, A. Holmen, Catal. Today 275 (2016) 11–19.

[6] T.P. Mokoena, E.C. Linganiso, H.C. Swart, V. Kumar, O.M. Ntwaeaborwa, Ceram. Int. 43 (2017) 174–181.

[7] X. Liang, X. Wang, Mater. Des. 112 (2016) 519–529.

[8] W.L. Suchanek, J. Am. Ceram. Soc. 93 (2010) 399–412.

[9] W.L. Suchanek, J.M. Garcés, P.F. Fulvio, M. Jaroniec, Chem. Mater. 22 (2010) 6564–6574.

[10] C. Wang, Y. Jia, Z. Zhang, G. Zhao, Y. Liu, Y. Lu, Appl. Surf. Sci. 478 (2019) 840–845.

[11] S.S. Punde, B.J. Tatarchuk, Appl. Catal. A 441–442 (2012) 54–64.

[12] J. Gascon, J.R. van Ommen, J.A. Moulijn, F. Kapteijn, Catal. Sci. Technol. 5 (2015) 807–817.

[13] A. Montebelli, C.G. Visconti, G. Groppi, E. Tronconi, C. Cristiani, C. Ferreira, S. Kohler, Catal. Sci. Technol. 4 (2014) 2846–2870.

[14] V. Paunovic, V. Ordomsky, M. Fernanda Neira D Angelo, J.C. Schouten, T.A. Nijhuis, J. Catal. 309 (2014) 325–332.

[15] S. Wahid, D.R. Cahela, B.J. Tatarchuk, AIChE J. 60 (2014) 3814–3823.

[16] A.V. Porsin, A.V. Kulikov, V.N. Rogozhnikov, A.N. Serkova, A.N. Salanov, K.I. Shefer, Catal. Today 273 (2016) 213–220.

[17] V. Novák, P. Kočí, T. Gregor, J. Choi, F. Štěpánek, M. Marek, Catal. Today 216 (2013) 142–149.

[18] J. Li, Y. He, L. Tan, P. Zhang, X. Peng, A. Oruganti, G. Yang, H. Abe, Y. Wang, N. Tsubaki, Nat.

Catal. 1 (2018) 787–793.

[19] H. Yue, Y. Zhao, X. Ma, J. Gong, Chem. Soc. Rev. 41 (2012) 4218–4244.

[20] S. Peng, Z. Xu, Q. Chen, Z. Wang, D. Lv, J. Sun, Y. Chen, G. Guo, ACS Catal. 5 (2015) 4410–4417.

[21] X. Gao, Y. Zhao, S. Wang, Y. Yin, B. Wang, X. Ma, Chem. Eng. Sci. 66 (2011) 3513–3522.

[22] S. Peng, Z. Xu, Q. Chen, Y. Chen, J. Sun, Z. Wang, M. Wang, G. Guo, Chem. Commun. 49 (2013) 5718–5720.

[23] C. Wang, L. Han, P. Chen, G. Zhao, Y. Liu, Y. Lu, J. Catal. 337 (2016) 145–156.

[24] C. Wang, L. Han, Q. Zhang, Y. Li, G. Zhao, Y. Liu, Y. Lu, Green Chem. 17 (2015) 3762–3765.

[25] C. Wang, W. Xu, Z. Qin, S. Mintova, Catal. Commun. 119 (2019) 39–41.

[26] M. Zhang, B. Xu, G. Ling, Appl. Surf. Sci. 331 (2015) 1–7.

[27] V. Maurice, G. Despert, S. Zanna, M.P. Bacos, P. Marcus, Nat. Mater. 3 (2004) 687–691.

[28] C. Kaplin, R. Ivanov, M. Paliwal, I. Jung, M. Brochu, Intermetallics 54 (2014) 209–217.

[29] K.R. Nemade, S.A. Waghuley, Ceram. Int. 40 (2014) 6109–6113.

[30] K. Laishram, R. Mann, N. Malhan, Ceram. Int. 38 (2012) 1703–1706.

[31] A.K.N. Kumar, S. Prasanna, B. Subramanian, S. Jayakumar, G.M. Rao, J. Appl. Phys. 117 (2015) 125307–125317.

[32] J.A. Rotole, P.M.A. Sherwood, Surf. Sci. Spectra 5 (1998) 4–10.

[33] J.A. Rotole, P.M.A. Sherwood, Surf. Sci. Spectra 5 (1998) 53–59.

[34] J. Sung Lee, H. Soo Kim, J. Su Lee, N. Park, T. Jin Lee, M. Kang, Ceram. Int. 38 (2012) 6685–6691.

[35] J.T. Kloprogge, L.V. Duong, B.J. Wood, R.L. Frost, J. Colloid Interface Sci. 296 (2006) 572–576.

[36] Z. Shi, W. Jiao, L. Chen, P. Wu, Y. Wang, M. He, Microporous Mesoporous Mater. 224 (2016) 253–261.

[37] X. Zhou, J. Ji, D. Wang, X. Duan, G. Qian, D. Chen, X. Zhou, Chem. Commun. 51 (2015) 8853–8856.

[38] G. Busca, Catal. Today 226 (2014) 2–13.

[39] P. Chang, F. Yen, K. Cheng, H. Wen, Nano Lett. 1 (2001) 253–261.

[40] M.I.F. Macêdo, C.A. Bertran, C.C. Osawa, J. Mater. Sci. 42 (2007) 2830–2836.

[41] H.J. Grabke, Intermetallics 7 (1999) 1153–1158.

[42] Z. Li, W. Wang, D. Yin, J. Lv, X. Ma, Front. Chem. Sci. Eng. 6 (2012) 410–414.

[43] C. Wang, P. Chen, Y. Li, G. Zhao, Y. Liu, Y. Lu, J. Catal. 344 (2016) 173–183.

[44] M. Sheng, H. Yang, D.R. Cahela, B.J. Tatarchuk, J. Catal. 281 (2011) 254–262.

[45] Y. Li, Q. Zhang, R. Chai, G. Zhao, Y. Liu, Y. Lu, F. Cao, AIChE J. 61 (2015) 4323–4331.